Progress In Electromagnetics Research M, Vol. 105, 205–217, 2021

Design of Compact Hexagonal Shaped Multiband Antenna for Wearable and Tumor Detection Applications

Navneet Sharma[1, *], Anubhav Kumar[1], Asok De[2], and Rakesh K. Jain[1]

Abstract—A compact multiband antenna for frequency bands of 2.45 GHz (ISM), 3.3 GHz (5G), and 5.8 GHz (ISM) is proposed. A modified Complementary Split Ring Resonator (CSRR) and cross-shaped stub are introduced in a hexagonal radiator to achieve triple-band operation including both ISM bands applications of 2.45 GHz, 5.8 GHz and WiFi/WLAN. The stubs in the radiator also improve the bandwidth and impedance matching of the antenna. The 10 dB impedance of the proposed antenna varies from 2.43 GHz to 2.64 GHz, 3.02 GHz to 3.85 GHz, and 4.88 GHz to 6.82 GHz. The antenna is analyzed on a human phantom model for wearable applications, where simulated SAR and theoretically calculated SAR are 0.3251 W/kg and 0.3299 W/kg, respectively. The antenna is used on a human breast model for cancer detection applications, where the SAR value is used to analyze and validate the performance of the antenna; therefore, the antenna has effectively worked for biomedical and wearable applications.

1. INTRODUCTION

Multiband, low cost antennas are in demand as they cater the need of present wireless communication system. Antennas capable of radiating in more than one band are particularly useful in wearable and handheld devices because the compact size of wearable devices does not allow integrating more than one antenna for several communication channels. In literature, many researchers have introduced compact microstrip multiband antennas with various design structures [1–10]. In [1], a hexagonal inset feed radiator is used for dual-band applications, where frequency selective surface increases the antenna gain. In [2], a CPW-fed antenna with tapered ground is designed with inner Split Ring Resonator(SRR) and an outer Close Ring resonator (CRR) to obtain dual bands. In [3], a modified circular loop radiator with partial ground is used to achieve the dual-band operation. In [4], a hexagonal CSRR is used with partial ground for dual-band operation. In [5], a metallic strip is used in the outer square of the patch and on feed for radiating equivalent magnetic current loop for upper and lower bands of a dual-band antenna. In [6], a dual-band miniaturized electrically small antenna is designed. In [7], two CSRRs are inserted in the radiator to achieve multiband operation. In [8], triangular resonators are used to achieve triple band operations with metamaterial characteristics. In [9], a CSRR is loaded on a radiator with partial ground to achieve dual-band operation. In [10], vertical and horizontal slots in antenna with offset-feed and full-ground are responsible for multiple bands. In [11], a meander line structure with offset-feed is used, where meander line dimensions are used to fine-tune the desired band. In [12], a pentagonal shape is etched on a square-shaped radiator, where a circular stub is accomplished with an E-shaped slot inside the radiator for wideband applications. The proposed antenna is designed by keeping in mind the wearable and biomedical applications, where compact antennas are required to be

Received 17 August 2021, Accepted 11 November 2021, Scheduled 26 November 2021

* Corresponding author: Navneet Sharma (navneet1979@gmail.com).

[1] Department of Electronics and Communication Engineering, Shobhit Institute of Engineering & Technology (Deemed to-be University), Meerut, (U.P.), India. [2] Department of Electronics and Communication Engineering, Delhi Technological University, Delhi, India.

incorporated with other wearable devices. The proposed antenna has multiband operation, and it is compact and has stable radiation in all the three bands. The antenna is suitable for 5G, wearable and cancer detection applications. The proposed antenna has the following novelty.

(i) The size of the antenna is compact, which could be easily incorporated in a wearable device with minimal effective area.

(ii) The antenna is tested over a human phantom model, where very low loading effect is observed.

(iii) The design is fabricated on low-cost and easily available FR-4 material; therefore, it can also be accomplished in compact and wearable devices.

(iv) The antenna is designed in such a way that it could cater both WiFi, ISM as well as 5G and WLAN Communication applications.

2. ANTENNA DESIGN AND EVOLUTION ANALYSIS

The multiband antenna with a compact and optimized geometry is designed on FR-4 material (ε_r= 4.4), and its hardware is represented in Fig. 1(a). The dimensional statistics of the metamaterial antenna is $30 \times 20 \times 1.6\,\text{mm}^3$. The optimized dimensions of antenna are as follows: $Wh = 30\,\text{mm}$, $Wb = 20\,\text{mm}$, $W1 = 10\,\text{mm}$, $r1 = 5.8\,\text{mm}$, $W2 = 9.5\,\text{mm}$, $r2 = 3.5\,\text{mm}$, $W3 = 3\,\text{mm}$, $W5 = 7.1\,\text{mm}$, $W4 = 0.5\,\text{mm}$ and $r3 = 5\,\text{mm}$.

The evolution of the antenna is discussed in three steps which is illustrated in Fig. 1(b). In step-1, a hexagonal radiator is used with partial ground where feed width is 3 mm to attain 50 Ω impedance. The 10 dB bandwidth of antenna varies from 2.62 GHz to 3.59 GHz as depicted in Fig. 1(c). In step-2, SRR with cross-shaped stub is integrated in the radiator to improve the impedance bandwidth (IBW) of the antenna, and dual operating bands are achieved. The 10 dB impedance bandwidth varies from 2.47 GHz to 3.12 GHz and 5.58 GHz to 6.93 GHz. In step-3, SRR with crossed stub is combined with outer radiator to improve the surface current, where the impedance bandwidth (IBW) of the antenna is enhanced. The 10 dB impedance bandwidth (IBW) at this step exists from 2.43 GHz to 2.64 GHz, 3.02 GHz to 3.85 GHz, and 4.88 GHz to 6.82 GHz, where it covers ISM and 5G bands. For metamaterial analysis, Nicolson Ross weir method is used to reveal the real values of permittivity (ε) and permeability (μ) as given by Equation (1) to Equation (5).

$$Permittivity(\varepsilon) = \frac{n}{z} \tag{1}$$

$$Permeability\,(\mu) = nz \tag{2}$$

where "n" is the refractive index, and "z" is the impedance, which is calculated using Equation (3) and Equation (4), respectively.

$$(n) = \frac{1}{k_0 L}\left\{\left[\text{Im}\left[\text{In}\,(A)\right] + 2m\pi\right] + j\text{Re}\left[\text{In}\,(A)\right]\right\} \tag{3}$$

$$(z) = \pm\sqrt{\frac{(1+S_{11})^2 - S_{21}^2}{(1-S_{11})^2 - S_{21}^2}} \tag{4}$$

The term "A" represents the absorption of metamaterial and is extracted by Equation (5).

$$(A) = \frac{S_{21}}{1 - S_{21}\dfrac{z-1}{z+1}} \tag{5}$$

where $|S_{21}|$ and $|S_{11}|$ are the transmission and reflection coefficients, respectively. It has been observed that permittivity is negative at lower resonant frequency at 2.55 GHz and permeability is negative at 3.3 GHz resonant frequency whereas permeability is approximately zero. Permittivity is close to zero, and permeability is negative at higher resonant frequency of 5.47 GHz as depicted in Fig. 1(d).

Electromagnetic property of the antenna changes with CSRR as the current distribution is disturbed; therefore, a band rejection notch is produced. The position of notch f_{notch} for single CSRR could be estimated by Equations (6) and (7) as

$$f_{\text{notch}} = \frac{c}{(L_{in} + L_{out})\sqrt{\varepsilon_T}} \tag{6}$$

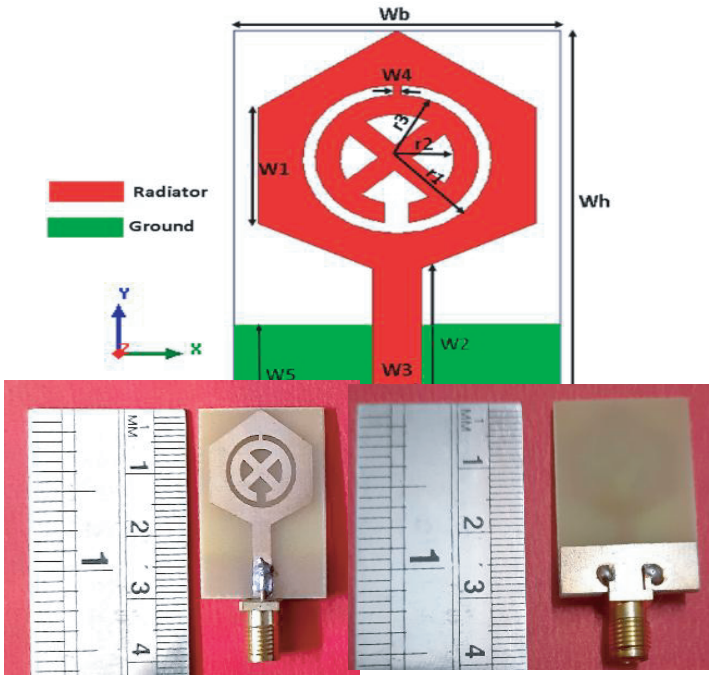
Wb
W4
W1
Wh
Radiator
Ground
Y
X
Z
W5
W3
W2

(a)

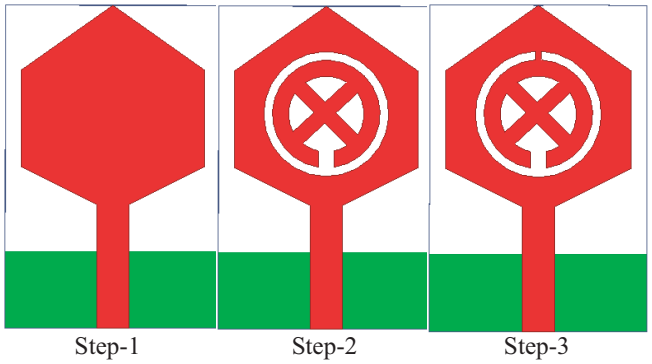
Step-1
Step-2
Step-3

(b)

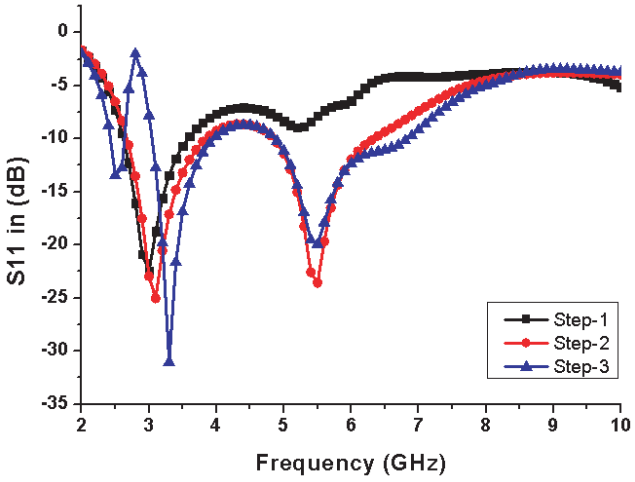
S11 in (dB)
Frequency (GHz)
Step-1
Step-2
Step-3

(c)

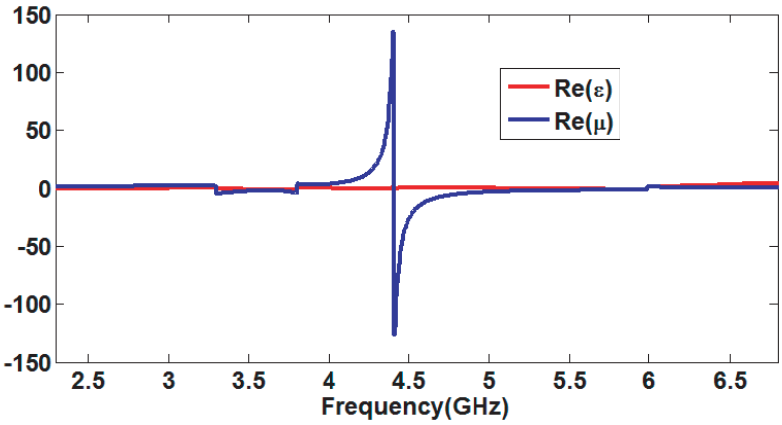

(d)

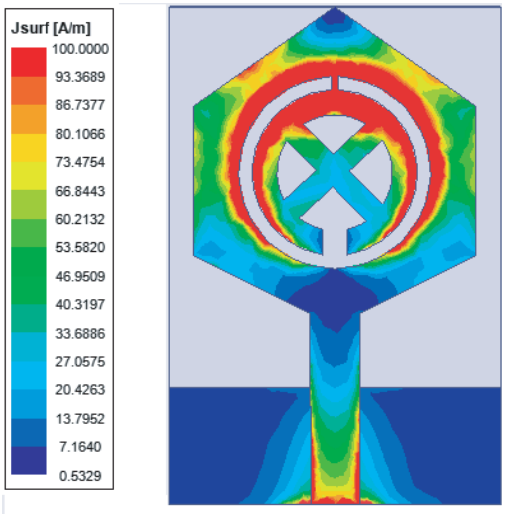

(e)

Figure 1. (a) Proposed multiband antenna and Fabricated prototype. (b) Evolution steps. (c) S_{11} parameters of evolution steps. (d) permittivity and permeability. (e) Current distribution at 2.81 GHz.

where,

$$\begin{aligned} L_{in} &= \text{inner length of CSRR} \\ L_{out} &= \text{outer length of CSRR} \\ c &= \text{speed of light.} \\ \varepsilon_T &= \frac{\varepsilon r + 1}{2} \\ \varepsilon_r &= \text{relative substrate permittivity} \end{aligned} \tag{7}$$

In the proposed design, the values of L_{in} and L_{out} are 29.91 mm and 34.94 mm, respectively. The frequency obtained from Equation (6) is 2.81 GHz thereby validating the notch at 2.81 GHz as depicted in Fig. 1(c). Fig. 1(e) depicts the current distribution at 2.81 GHz.

3. SAR ANALYSIS OF ANTENNA ON HUMAN PHANTOM MODEL

As the antenna is positioned in proximity with human body, the antenna performance varies due to lossy characteristics of human body. The antenna performance is analyzed on a four-layered human phantom model where the phantom model is placed at 15 mm distance from the antenna ground. The four layers

of human phantom are composed of skin (dry), fat, muscles, and bone (cortical) with thicknesses 2 mm, 3.5 m, and 10 mm, respectively [15] as depicted in Fig. 2(a).

Parametric values of the tissues such as relative permittivity, mass conductivity, and loss tangent change with the operating frequency as depicted in Table 1. The antenna parameters are analyzed at 5.8 GHz, where the parameters are approximately the same as when the electrical characteristics of phantom model are used for 2.4 GHz and 3.3 GHz [14].

Table 1. Characteristic Values of human body tissues at 2.4 GHz, 3.3 GHz and 5.8 GHz [14].

Tissue Name	Frequency (GHz)	Relative Permittivity (ε_r)	Conductivity (S/m)	Loss Tangent (σ)
Skin	2.4	38.0	1.464	0.283
Fat		5.280	0.1045	0.145
Muscle		52.729	1.7388	0.24194
Bone		11.381	0.39431	0.2542
Breast Fat		5.1563	0.13344	0.19382
Skin	3.3	37.179	1.9074	0.27946
Fat		5.1938	0.14509	0.15217
Muscle		51.691	2.386	0.25144
Bone		10.901	0.5706	0.28513
Skin	5.8	35.114	3.717	0.32807
Fat		4.9549	0.29313	0.18335
Muscle		48.485	4.9615	0.31715
Bone		9.6744	1.1544	0.36981

It is observed that the 10 dB IBW has a minor effect due to the presence of human phantom model where efficiency is reduced from 95% to 66 % by the presence of phantom model. The gain enhancement in antenna is observed from 1.28 dB to 3.14 dB at 2.4 GHz, from 2.21 dB to 3.63 dB at 3.3 GHz and from 3.6 dB to 5.2 dB at 5.8 GHz using phantom model. This shows that the gain with phantom is enhanced due to the reflection of grating lobes from the phantom model. SAR analysis is performed to study the effect of antenna radiation on the human phantom. When the antenna is used as a wearable device, the value of SAR should be lower than the prescribed limit of 1.6 W/kg on 1 g of standard human tissue. The observed SAR values are 0.32 W/kg, 0.47 W/kg, and 0.55 W/kg at 2.4 GHz, 3.3 GHz, and 5.8 GHz, respectively, as illustrated in Figs. 2(b), 2(c), and 2(d) when 10 mW power is incident to the antenna on 1 g standard human phantom. Table 2 depicts the simulated and theoretically calculated values of SAR. The $|S_{11}|$, realized gain, and radiation efficiency with and without phantom model of proposed antenna are illustrated in Figs. 2(e), 2(f), and 2(g).

Table 2. Comparison of simulated and theoretical calculations of SAR in human phantom model.

Frequency (GHz)	**Simulated SAR (W/kg)**	**Theoretically Calculated SAR (W/kg)**
2.4	0.3251	0.3299
3.3	0.4758	0.4764
5.8	0.5583	0.5605

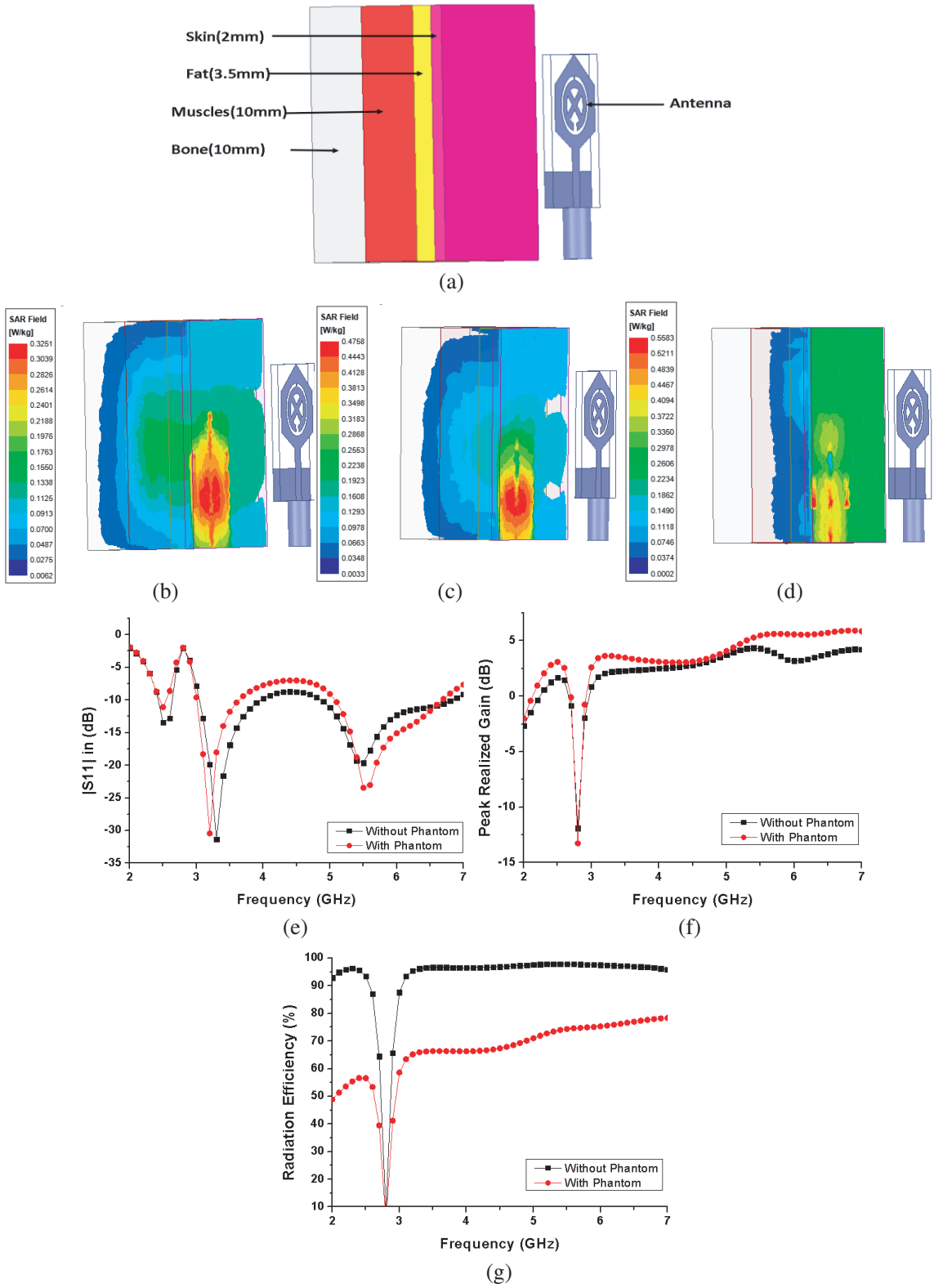

Figure 2. (a) Antenna placed on 4-layered human phantom. (b) SAR analysis at 2.4 GHz. (c) SAR analysis at 3.3 GHz. (d) SAR analysis at 5.8 GHz. (e) $|S_{11}|$ with and without phantom model. (f) Peak Realized Gain with and without phantom model. (g) Radiation efficiency with and without phantom model.

4. DETECTION OF TUMOR BASED ON SAR ANALYSIS

4.1. Female Breast Model Design

Tumors in human female breasts are quite common these days, and it is necessary that the tumor is detected at early stages so that immediate medical attention could be provided. The tumor detection technologies that are conventionally available are expensive and complicated.

It is observed that the occurrence of tumor changes the relative permittivity and conductivity of the tissues near the tumor, thereby altering the $SAR_{(average)}$ values. The presence of tumor could be detected by the analysis of $SAR_{(average)}$ values of human female breast tissues that contain tumor, and they are compared with healthy breast tissues. For this purpose, SAR analysis is performed at 2.45 GHz ISM band. The parameters of skin, breast fat, glandular cells, and tumor are appropriately chosen in accordance to the frequency used [13, 14] as given in Table 1. Table 3 depicts the $SAR_{(average)}$ values and the difference of $SAR_{(average)}$ in all the tissues, and Table 4 gives the SAR of the tumor at 2.45 GHz.

Table 3. $SAR_{(average)}$ values of tissue types at 2.45 GHz.

SAR Analysis with/without tumor at 2.45 GHz				
Tissue type		**With Tumor**	**Without Tumor**	**SAR difference**
Skin	**Max**	271.21	299.8	28.59
	Min	0.0219	0.156	0.1341
Breast Fat	**Max**	26.083	29.019	2.936
	Min	0.0151	0.0277	0.0126
Glandular Cell	**Max**	6.4243	8.279	1.8547
	Min	0.0151	0.12	0.0645
Tumor Cell	**Max**	7.7461	-	-
	Min	4.7165	-	-

Table 4. Simulated and theoretically calculated SAR of female breast phantom model.

Tissue	**Simulated SAR (W/kg)**		**Theoretically calculated SAR (W/kg)**	
	With Tumor	**Without Tumor**	**With Tumor**	**Without Tumor**
Skin	271.21	299.8	273.3704	304.825573
Breast Fat	26.083	29.019	26.32955	30.8124
Glandular Cells	6.4243	8.279	7.1439	8.5419

4.2. Specific Absorption Rate (SAR)

When radiation from the antenna is subjected to human body, certain part of this radiation is absorbed by the tissues. Therefore, SAR is the power in Watts (W) that a unit mass of 1 kilogram of tissue absorbs, averaged at 1 g or 10 g of human tissue given by Equation (1).

$$\mathrm{SAR}_{\mathrm{average}}(r,\omega) = \frac{1}{V}\int \frac{\sigma(r,\omega)\,|E(r,\omega)|_2}{2\rho(r)}dr$$

where,

$$\begin{aligned}(r,\omega) &= \text{Conductivity in Siemens/Meter}\\ r &= \text{Position of Vector}\\ V &= \text{Volume in meter cube}\end{aligned}$$

$$\sigma = \text{Electrical Conductivity (sample)}$$
$$\rho = \text{Density (Sample)}$$
$$|E(r,\omega)|_2 = \text{Electrical field in Volts/meter}$$

4.3. Analysis of Tumor on Female Breast Model

To analyze the cancer detection of a human breast model, two theories are suggested based on the difference of SAR at 2.4 GHz when 2 W input power is incident to the antenna at 1 g standard human tissue. In the first theory, the $SAR_{1\,g}$ values of skin tissue, breast fat, and glandular tissue are evaluated. The $SAR_{1\,g}$ (Max) values without tumor are evaluated to be 299.8040 W/kg, 29.0192 W/kg, and 8.2750 W/kg, respectively, whereas the $SAR_{1\,g}$ (Max) values with tumor are 271.2186 W/kg, 26.0832 W/kg, and 6.4243 W/kg. Thus the SAR differences of 28.59 W/kg, 2.936 W/kg, and 1.8547 W/kg are observed at skin tissue, breast fat, and glandular tissue, respectively. In the second theory, the differences in the SAR values (Max and Min) of tumor and surrounding glandular cell are analyzed. It has been observed that the maximum and minimum values of $SAR_{(average)}$ on glandular tissue are 6.4243 W/kg and 0.0151 W/kg. The maximum and minimum values of $SAR_{(average)}$ for tumor are 7.7461 W/kg and 4.7165 W/kg; therefore, it is clearly revealed that SAR difference is observed between tumor tissue and its surrounding glandular tissue. The distance of antenna from human female breast model is 3 mm, and the antenna is positioned close enough for the radiation to produce maximum SAR difference.

An analysis of the SAR values of different tissues (simulated and theoretically calculated) is given in Table 4. It is observed that the simulation results match the theoretically calculated values. Table 5 gives the effect of SAR on tumor size, and it has been observed that on increasing the size of tumor, the SAR value decreases in skin and breast fat tissues, but SAR values of glandular cell and tumor are increased. The SAR of tumor increases if the tumor is located close to antenna, which is revealed in Table 6. As tumor gets older, its mass density increases due to the accumulation of blood and other fluids, and it is evident from Table 7, which shows that SAR values decrease with increase in mass

Table 5. SAR analysis on different size of tumor.

Tissue/Size	**Radius: 4 mm**	**Radius: 8 mm**	**Radius: 12 m**
Skin	294.9395	271.2186	247.4847
Fat	40.3011	26.0832	17.2234
Glandular Cells	4.6606	6.4243	8.7176
Tumor	5.2341	7.7461	9.4377

Table 6. SAR analysis on different position of tumor.

Position of tumor from antenna and SAR in W/kg					
Location from Antenna	**50 m**	**45 mm**	**40 mm**	**35 mm**	**30 mm**
Max	0.945	2.6545	7.7461	23.1214	66.7214
Min	0.502	1.3543	4.7165	11.1544	32.0373

Table 7. SAR analysis on different mass density of tumor.

SAR in W/kg with Change in Mass Density in kg/^{m3} of Tumor			
Mass Density	**900**	**1000**	**1100**
Max	8.2801	7.7461	7.2573
Min	4.069	4.7165	3.3341

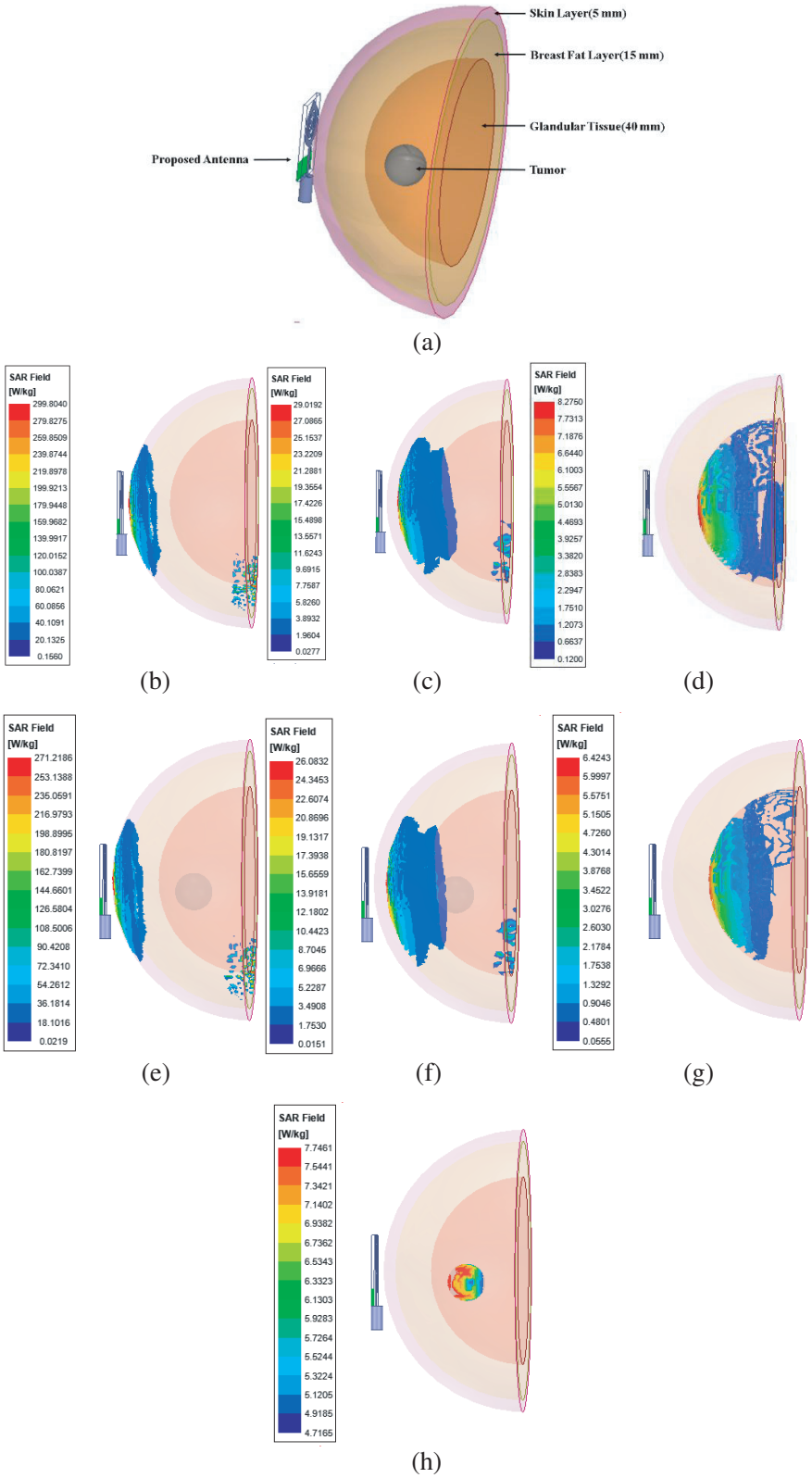

Figure 3. (a) 3D Model of human female breast. (b) SAR analysis of skin tissue without tumor. (c) SAR analysis of breast fat tissue without tumor. (d) SAR analysis of glandular cell without tumor. (e) SAR analysis of skin tissue with tumor. (f) SAR Analysis of breast fat tissue with tumor. (g) SAR analysis of glandular tissue with tumor. (h) SAR analysis of tumor.

density. The simulated human female breast model is depicted in Fig. 3(a). The SAR analyses of skin, fat, and glandular tissue without tumor are depicted in Figs. 3(b), 3(c), and 3(d), whereas SAR analyses of skin, fat, and glandular tissue with tumor are illustrated in Figs. 3(e), 3(f), and 3(g). The SAR analysis of tumor is shown in Fig. 3(h).

5. RESULTS AND DISCUSSIONS

The proposed three-band antenna for a wearable device is measured on Anritsu, Virtual Network Analyzer (VNA) (MS2038C) to validate the measured results in an anechoic chamber. The $|S_{11}|$ (in dB) of proposed antenna is achieved from 2.43 GHz to 2.64 GHz, 3.02 GHz to 3.85 GHz, and 4.88 GHz to 6.82 GHz as depicted in Fig. 4(a). The realized gain and efficiency (simulated) of multiband antenna are illustrated in Figs. 4(b) and 4(c), where the gain varies from 1.28 dB to 4.20 dB, and efficiency is above 90% throughout the operating band. The normalized radiation patterns of antenna at resonant frequency in different planes are illustrated in Figs. 4(d), 4(e), and 4(f) where stable radiation pattern is achieved with more than 20 dB difference in cross- and co-polarizations. The proposed multiband antenna can be used for wearable and biomedical applications and is applicable to Wi-Fi/WLAN, ISM

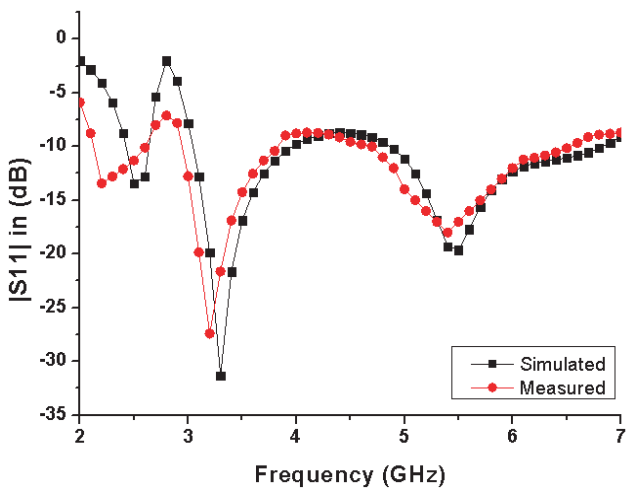

(a)

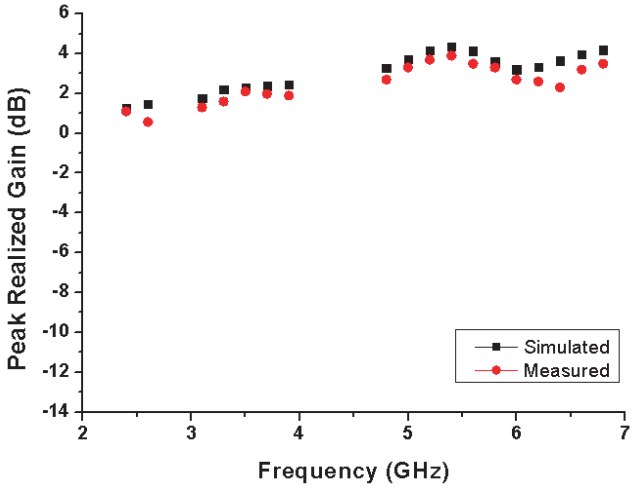

(b)

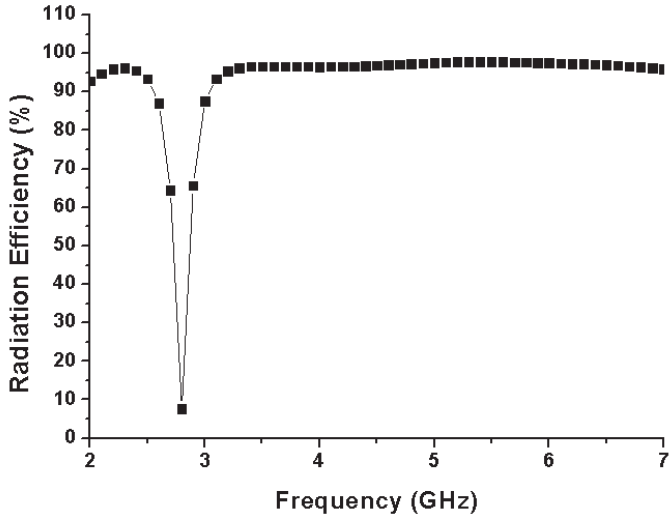

(c)

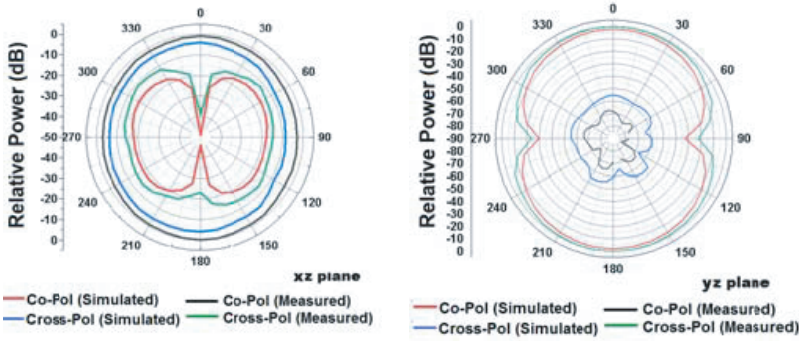

(d)

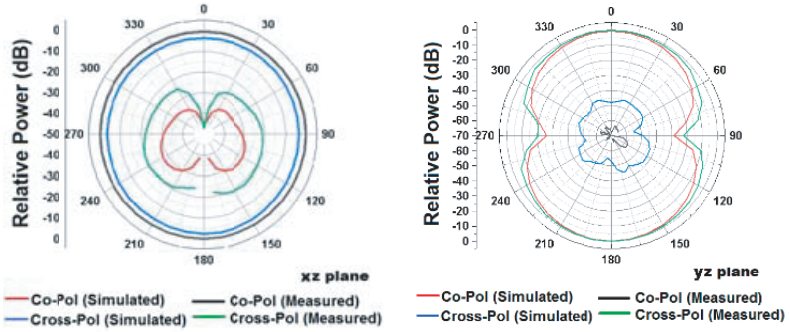

(e)

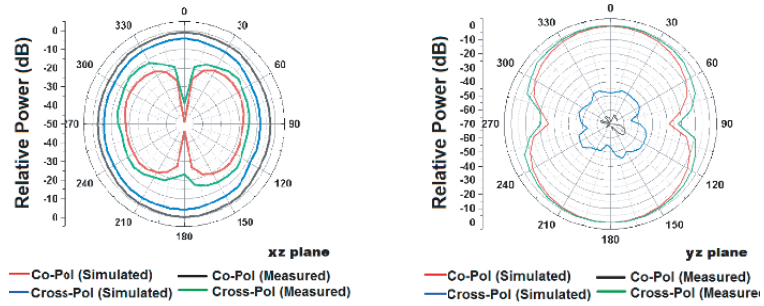

(f)

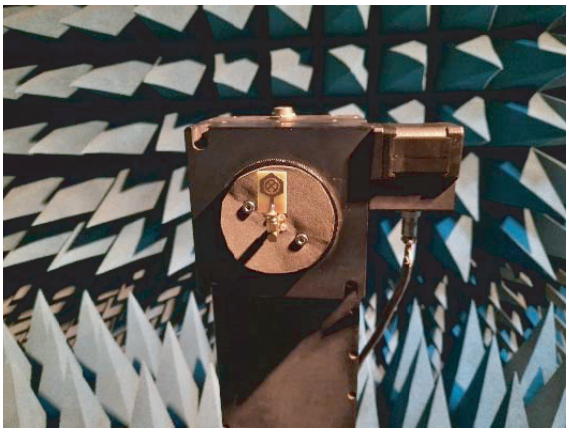

(g)

Figure 4. Simulated and measured results of multiband antenna. (a) $|S_{11}|$ in dB. (b) Peak realized gain (dB). (c) Radiation efficiency. (d) Radiation patterns (normalized) in xz and yz planes (2.4 GHz). (e) Radiation patterns (normalized)in xz and yz planes (3.3 GHz). (f) Radiation patterns (normalized)in xz and yz planes (5.8 GHz). (g) Measurement of antenna in anechoic chamber.

Table 8. Comparative analysis of published papers with proposed work.

Ref.	Size (mm)	10 dB (GHz)	No. of Bands	Gain (dB)
[1]	35 × 28	5.7, 10.3	2	5.26, 4.85
[2]	31.7 × 27	2.6–2.6 and 3.2–4.2	2	0.532–1.441, 1.981–1.983
[3]	30 × 30	1.88–7.0, 7.81–8.85 and 9.6–14.3	3	1.62, 1.77, 3.18
[4]	30 × 30	2.42–2.60, 3.44–5.84	2	0.66, 1.72
[5]	52 × 32	2.67–3.40, 3.61–3.67	2	0.15–3.81, 3.47–3.75
[6]	50 × 12	1.88–1.90, 2.25–3.50	2	−0.67, 2.3
[7]	27 × 25	2.4, 3.5 and 5.0	3	2.46
[8]	35 × 38	1.78–1.84, 2.34–3.86 and 5.75–5.87	3	NG
[9]	50 × 50	1.61–1.84, 2.08–2.5	2	1.8, 1.6
Proposed Work	20 × 30	2.4, 3.3, 5.8	3	1.8, 2.5, 3.4

(2.4 GHz and 5.8 GHz) as well as Wi-Fi/WLAN. In Table 8, a comparative analysis is illustrated with proposed antenna and other multiband antenna, where the proposed antenna is compact in size and works in three operating bands of 2.4 GHz and 5.8 GHz ISM band as well as 5G band. It is observed that there is a marginal difference between the simulated and measured characteristics. The measured results have minor deviations due to soldering and fabrication, primarily occurring in compact antenna.

6. CONCLUSION

In this paper, a hexagonal radiator is used with a CSRR and cross-shaped stub for triple band applications. For improvement in impedance matching of the antenna and enhancing the operating bandwidth the CSRR and cross-shaped stub are used. The SAR is evaluated at different resonant frequencies for wearable applications, where it validates the antenna performance. The cancer detection analysis by using proposed antenna is discussed in this paper, where cancer detection is observed with variations in SAR.

ACKNOWLEDGMENT

The antenna is designed and simulated on HFSS-19 at the "Optical, Antenna and Microwave Engineering" facility at ABES Engineering College, Ghaziabad.

REFERENCES

1. Rajak, N., N. Chattoraj, and R. Mark, "Metamaterial cell inspired high gain multiband antenna for wireless applications," *AEU — International Journal of Electronics and Communications*, Vol. 109, 23–30, 2019.
2. Si, L.-M., W. Zhu, and H.-J. Sun, "A compact, planar, and CPW-fed metamaterial-inspired dual-band antenna," *IEEE Antennas and Wireless Propagation Letters*, Vol. 12, 305–308, 2013.
3. Sharma, N. and S. S. Bhatia, "Metamaterial inspired fidget spinner-shaped antenna based on parasitic split ring resonator for multi-standard wireless applications," *Journal of Electromagnetic Waves and Applications*, Vol. 34, No. 10, 1471–1490, 2020.

4. Murugeshwari, B., R. Samson Daniel, and S. Raghavan, "A compact dual band antenna based on metamaterial-inspired split ring structure and hexagonal complementary split-ring resonatorfor ISM/WiMAX/WLAN applications," *Applied Physics A*, Vol. 125, No. 9, 1–8, 2019.
5. Hasan, M. M., M. R. I. Faruque, and M. T. Islam, "Dual band metamaterial antenna for LTE/bluetooth/WiMAX system," *Scientific Reports*, Vol. 8, No. 1, 1–17, 2018.
6. Sharma, S. K., M. A. Abdalla, and Z. Hu, "Miniaturisation of an electrically small metamaterial inspired antenna using additional conducting layer," *IET Microwaves, Antennas & Propagation*, Vol. 12, No. 8, 1444–1449, 2018.
7. Rajeshkumar, V. and S. Raghavan, "A compact metamaterial inspired triple band antenna for reconfigurable WLAN/WiMAX applications," *AEU — International Journal of Electronics and Communications*, Vol. 69, No. 1, 274–280, 2015.
8. Zhu, C., et al., "Electrically small metamaterial-inspired tri-band antenna with meta-mode," *IEEE Antennas and Wireless Propagation Letters*, Vol. 14, 1738–1741, 2015.
9. Sharma, S. K. and R. K. Chaudhary, "Dual-band metamaterial-inspired antenna for mobile applications," *Microwave and Optical Technology Letters*, Vol. 57, No. 6, 1444–1447, 2015.
10. Patel, R., et al., "Meandered low profile multiband antenna for wireless communication applications," *Wireless Networks*, Vol. 27, No. 1, 1–12, 2021.
11. Patel, R., et al., "Low profile multiband meander antenna for LTE/WiMAX/WLAN and INSAT-C application," *AEU — International Journal of Electronics and Communications*, Vol. 102, 90–98, 2019.
12. Girjashankar, P. R., T. Upadhyaya, and N. Daftary, "Design of dual wideband planar antenna for wireless applications," *2019 Third International Conference on I-SMAC (IoT in Social, Mobile, Analytics and Cloud)(I-SMAC)*, IEEE, 2019.
13. Subramanian, S., B. Sundarambal, and D. Nirmal, "Investigation on simulation-based specific absorption rate in ultra-wideband antenna for breast cancer detection," *IEEE Sensors Journal*, Vol. 18, No. 24, 10002–10009, 2018.
14. nst. of Appl. Phys., Italian Nat. Res. Council, "Calculation of the dielectric properties of body tissues in the frequency range 10 Hz–100 GHz," Florence, Italy, [Online], Available: http://niremf.ifac.cnr.it/tissprop.
15. Karthik, V. and T. Rama Rao, "Investigations on SAR and thermal effects of a body wearable microstrip antenna," *Wireless Personal Communications*, Vol. 96, No. 3, 3385–3401, 2017.